On the influence of bed roughness on saltation in inertial regime

Gaspard Minster, France Floc'H, Alexandre Valance, Nicolas Le Dantec, Amandine Nicolle, Benoit Zerr

Received: 28 February 2023 | Revised: 8 December 2023 | Accepted: 22 December 2023

DOI: 10.1002/esp.5767

RESEARCH ARTICLE

ESPL WILEY

On the influence of bed roughness on saltation in inertial regime

Gaspard Minster[1,5] | France Floc'h[2] | Alexandre Valance[3] | Nicolas Le Dantec[2] | Amandine Nicolle[1,4] | Benoit Zerr[1,5]

[1]ENSTA-Bretagne, Brest, France

[2]Univ Brest, CNRS, Geo-Ocean UMR 6538, Plouzané, France

[3]Institut de Physique de Rennes, CNRS, UMR 6251, Univ Rennes, Rennes, France

[4]Station Biologique de Roscoff, Laboratoire Adaptation et Diversité-en Milieu Marin (AD2M), UMR 7144, Roscoff, France

[5]Lab-STICC, CNRS, UMR 6285, Brest, France

Correspondence
France Floc'h, Univ Brest, CNRS, Geo-Ocean UMR 6538, F-29280 Plouzané, France.
Email: France.floch@univ-brest.fr

Funding information
Agence Nationale de la Recherche, Grant/Award Numbers: ANR-10-IEED-0006-10, ANR-17-EURE-0015; Investissements d'Avenir

Abstract

In extreme tidal environment, occurrences of saltating pebbles have been observed. The ambition to instal hydrokinetic turbines in such environment requires knowledge on the presence of pebbles in saltation in the water column because they can damage the structures. An experimental study is realized in a free-surface flume with no slope and different bed roughnesses as in marine environment. With fast camera the trajectories of hundreds of spherical particles are analysed. Our study deals with saltation in the inertial regime (i.e., large Stokes number) over fixed beds with various roughnesses. In inertial regime, the bed roughness has more influence on the collision process and the trajectory of the particles than for non-inertial motion where viscous forces play a key role. Jump height and length increase with bed roughness, with height increasing quicker than length leading to a more vertical trajectory for higher bed roughness. The vertical restitution coefficient is shown to increase with bed roughness leading to higher jumps. The initiation of the motion is shown to depend on the bed roughness as well. Power laws of the excess shear stress are proposed for jump height and length, taking into account the bed roughness. The dataset and analysis proposed in this study is a key ingredient for developing quantitative models for particle transport.

KEYWORDS
bed roughness, coarse sediment, critical Shields, inertial regime, saltation

1 | INTRODUCTION

Hydrokinetic power, generated by turbines submerged in seas and rivers experiencing intense currents, have a high potential for the production of renewable energy. To maximize energy production, hydrokinetic turbines in the marine environment are placed at locations with extreme tidal currents (up to 5 m/s). Under these conditions, coarse sediments with diameter greater than a few centimetres (5–20 cm) can be transported by the flow in saltation. It has been shown that coarse particles as pebbles can damage the structures up to 1 m above the bottom (Blanpain, 2009). The installation of hydrokinetic turbines thus offers new scientific challenge in understanding the sediment dynamics in extreme currents (Cada et al., 2007; Rahim & Stevens, 2013). The study of particle transport, in particular saltation motion, in the context of strong currents is the purpose of this paper.

Saltation transport (i.e., hopping motion) is part of the bedload, with the rolling and sliding motions. Bedload concerns the transport of particles that remain in contact with the bed surface. In saltation, under the effect of fluid drag, the particles detach from the bed to experience ballistic-like trajectories. Unlike suspension, the gravitational force is dominant, so that saltating particles return to the bed. Importantly, in bedload regime (e.g., in saltation), the horizontal velocity of the particles may differ from the horizontal flow velocity. Saltation occurs concomitantly with rolling, the proportion of each varying according to the flow strength (Abbott & Francis, 1977). The jump (i.e., hop) parameters (height, length, velocity and trajectory) are determined by the strength of the flow for a given grain size and are independent of grain density and stream depth (Abbott & Francis, 1977).

Sklar and Dietrich (2004) have shown using many different dataset (Abbott & Francis, 1977; Fernandez Luque & Van Beek, 1976;

Francis, 1973; Hu & Hui, 1996; Lee & Hsu, 1994; Niño et al., 1994; Sekine & Kikkawa, 1992; Wiberg & Smith, 1985b) that the height H and length L of saltation trajectories can be well approximated by power laws of the excess shear stress. Auel et al. (2017a) propose similar power laws but with different parametric values, using a wide range of their own and additional datasets (Ancey et al., 2002; Chatanantavet, 2007; Chatanantavet et al., 2013; Ishibashi, 1983; Lajeunesse et al., 2010; Niño & Garcìa, 1998; Ramesh et al., 2011). The general trend is the same: height and length both increase with increasing flow strength, but the increase is less pronounced for Auel et al. (2017a). The difference may be explained by the fact that Auel et al. (2017a) consider a wider range of experimental conditions, including subcritical and supercritical flow conditions, as well as various bed boundary conditions. Nonetheless, for both relationship, the uncertainty on the mean jump height prediction remain more than one order of magnitude and few dataset relating experiments with coarse particles (of several centimetres) are taken into account.

Over natural beds, rough turbulent regime dominates, for particle Reynolds number $R^* = du^*/\nu_f > 70$ (where d is the particle size, u^* the shear velocity and ν_f the kinematic viscosity of the fluid). In order to characterize the behaviour of a particle in a fluid, a Stokes number is used as $St = \sigma Re_p/18$ with the Reynolds number of fall particle $Re_p = \sqrt{gd^3(\sigma-1)/\sigma/\nu_f}$, with g the gravity acceleration and σ the density ratio of particles and fluid (Berzi et al., 2016; Delannay et al., 2017; Valance & Berzi, 2022). A particle with a large Stokes number is dominated by its inertia. In the inertial regime, $St > 500$, the particle motion is dominated by gravity forces, with viscous effect becoming negligible. Saltation motion is expected to be favoured in high Stokes number regimes, because the dissipation due to the viscous force is expected to be negligible during the collision with the bed, comparable with collision in the air (Gondret et al., 2002). A central issue is to understand the influence of bed roughness on the characteristics of the saltation trajectories, especially when the bed roughness length is different than the saltating particles diameter.

The role of the bed roughness was investigated by Bhattacharyya et al. (2013) using fixed beds with different roughnesses. Their experimental outcomes suggest that the larger the bed roughness, the higher the fluid shear stress required to sustain saltation motion. They also showed that for a given flow velocity, an increase in the bed roughness leads to an increase in the jump length and height. They interpret this result mainly as a hydrodynamic effect: rougher bed leads to larger bed shear stress. Auel et al. (2017a) conducted experiments on smooth beds and indicated that saltating particle trajectories were rather flat and elongated compared with alluvial beds. Recently, Demiral et al. (2022) have suggested that saltation trajectories are more vertical with increasing bed roughness. Thus the bed roughness would tend to change the length-to-height ratio of the trajectory.

The trajectory depends on the collision process: the impact can be characterized by the effective coefficient of restitution, which corresponds to the ratio of the rebound velocity to the impact velocity. This restitution coefficient thus evaluates the energy dissipation during the collision. Experimental measurements by Niño and Garcìa (1998) indicate that the restitution coefficient decreases with increasing Shields number, suggesting that the lubrication force plays a key role in the impact (Gondret et al., 2002). Gondret et al. (2002) investigated the head-on collision of spherical particles onto a flat plate in an quiescent fluid and showed that the effective restitution coefficient is an increasing function of the Stokes number: It equals zero at small Stokes numbers and reaches an asymptotic value at high Stokes numbers (between 0.65 and 0.98 depending on the material), corresponding to the classical 'dry' value when measured in air or vacuum. Joseph and Hunt (2004) and Beladjine et al. (2007) investigated oblique collision of particles onto a granular bed in air. They showed that the effective restitution coefficient linearly depends on the sinus of the impact angle θ_i. Grazing impacts are less dissipative than head-on impacts. We then investigate how the bed roughness modifies the impact angle and subsequently the restitution of energy.

In order to improve bedload formulae, including saltation at different vertical positions above the bed, the transition between rolling and saltation motions is also a crucial issue. The generally accepted idea is that the majority of the particles roll for Shields number close to incipient motion and that saltation become predominant as the Shields number increases (Van Rijn, 1984a). Hu and Hui (1996) suggest that saltation is the main mode of sedimentary transport in most flow conditions whereas Abbott and Francis (1977) clearly indicate that both types of motion are obtained in varying proportions for given dimensions of particle trajectories. A long-debated issue in sediment transport concerns the threshold for incipient motion. This threshold is characterized by the Shields number, that is, the dimensionless shear stress $\tau^* = u*^2/(gd(\sigma-1))$. The critical Shields number associated to the initiation of particle movement is not uniquely defined. A large variety of criteria and methods can be employed to assess incipient motion. In turbulent flows, for particle Reynolds number $R^* > 70$, the critical Shields number is constant and about 0.06 (Dancey et al., 2002; Dey, 2003; Rouse, 1939; Shields, 1936; Papanicolaou et al., 2002; Vanoni, 1975). However, extension of Shields work showed that values for mobile beds may vary from 0.025 to 0.086 (Buffington et al., 1992). As well for coarse sediment, Neill and Yalin (1969) and Gessler (1970) have shown that Shields original value ($\tau_c^* = 0.06$) would be overestimated by a factor 2. For fixed smooth beds, critical values are much lower and falls down to 0.007 (Hu & Hui, 1996) or even 0.005 on mortar (Auel et al., 2017a). Recently, Demiral et al. (2022) have shown an increased critical value for increasing roughness as well.

So this study deals with the influence of bed roughness on the saltation transport mode in inertial regime: experiments are conducted to study with large particles (several centimetres) in the regime of high particle Reynolds numbers ranging from 1000 to 5000 (and St from 700 to 4000), on fixed beds with varying roughness (of several centimetres). This provides unusual experimental conditions in comparison with the literature. Most experiments conducted in flumes have particle Reynolds number lower than 1000 (Abbott & Francis, 1977; Ancey et al., 2002; Bhattacharyya et al., 2013; Francis, 1973; Fernandez Luque & Van Beek, 1976; Hu & Hui, 1996; Lajeunesse et al.2010; Lee & Hsu, 1994; Niño & Garcìa, 1998; Ramesh et al., 2011; Sekine & Kikkawa, 1992; Wiberg & Smith, 1985a). Only a few experimental studies consider higher particle Reynolds numbers (Auel et al., 2017a; Chatanantavet et al., 2013; Ishibashi, 1983; Niño et al.1994).

Because characterizing the saltation regime in natural streams is challenging due to the difficulty to acquire data in hostile environments, conducting experiments in a flume is an alternative solution to study saltation and to mimic in a controlled way various natural situations. Since the first studies of sediment transport in a flume, which

appeared in the early 20th century (Gilbert & Murphy, 1914), data acquisition and flow measurement methods have evolved but have remained based on image capture analysis (Abbott & Francis, 1977; Auel et al., 2017a; Niño et al., 1994). This is the approach we follow here, using a high-speed camera.

2 | EXPERIMENTAL SET-UP AND IMAGE ANALYSIS

2.1 | Experimental set-up

The experimentation was conducted in the flume facility of the 'Institut de Physique de Rennes' (IPR) in Rennes (France). Experiments were carried out in a free-surface flume 40 cm wide, 60 cm height and 500 cm long (see Figure 1). The flume is equipped with pumps able to produce in practice a maximal flow discharge of 45 L/s. Three different flow rates were prescribed for our experiments: 11, 25 and 45 L/s. A honeycomb structure was placed at the beginning of the flume in order to break the large turbulent structures. The hydraulic slope of the flume was negligible, about 0.0001. Bed roughness consisted of spherical particles of uniform size glued on 3-m-long steel plates that were placed at the bottom of the channel, starting 1.5 m downstream of the honeycomb (Figure 1). The choice of glue was based on resistance tests. The requirements to be respected are to stick to both stainless steel and glass, to hold underwater and to have a hard fixation in order to avoid any phenomenon of damping which would distort the measurements by introducing an absorption factor. By considering these three imperatives, Araldite or a derivative has been used. The particles were densely packed according to a random arrangement (non-crystalline structure). Characterizing the bed roughness with the diameter of the glued particles d_B, three different bed roughnesses were used: $d_B = 1.2$,1.6 and 2.6 cm leading to nine configurations of different flows and bed types (Table 1). For all nine experiments, the flow depth h is measured along the flume (between 8 to 11 cm above the roughness depending on the experimental conditions), leading to d_B/h from 0.1 to 0.325 and a width-to-depth ratio l/h from 3.7 to 5.1 (Table 1). The Froude number $Fr = U_\infty/\sqrt{gh}$ is from 0.73 to 1.03.

2.2 | Flow profiles

The vertical profiles of mean velocity component u illustrate the characteristic features of the flow over the rigid-bed surface. A streamflow velocity meter Nixon 403 was used to measure the velocity profile. The instrument provides a 10 s averaged flow data every second. Five minutes of data has been used to get a mean flow velocity and a standard deviation. As the width-to-depth ratio in our present experimental set-up was about 4, there was uncertainty in the generation of secondary currents (Albayrak & Lemmin, 2011; Demiral et al., 2022). Therefore, we checked the flow for secondary currents. The lateral velocity throughout the flow depth was less than 5% of the stream-wise velocity component, and thus, the generation of secondary currents remains weak. For different flow conditions and bed roughness, velocity measurements have been performed at different positions along the flume. The velocity profiles are steady and stable all over the flume 10 min after having switch the system on. The surface flow velocities U_∞ are measured as 65, 85 and 107 cm/s for the prescribed flow rates 11, 25 and 45 L/s, respectively, whatever the bed roughness. The stream-wise normalized mean velocity $u^+(=u/u*)$ profile located in the centreline of the flume exhibited the standard log-law (wall law) over the plane/rough beds, with a range of regression coefficient R^2 from 0.80 to 0.95 (Figure 2).

Thus, the shear velocity u_* and hydraulic bed roughness y_0 were derived from these velocity profiles using the standard log-law:

$$u(z) = \frac{u^*}{\kappa} \ln \frac{y}{y_0}, \tag{1}$$

where κ is the von Karman constant ($\kappa \simeq 0.41$). In the hydraulically rough regime, the hydraulic roughness is related to the geometrical roughness of the bed and thus to the particle bed diameter d_B (Czernuszenko, 2011). Nikuradse (1933) established that the origin of velocity is $y_0 = k_s/30$ (where k_s is the roughness length scale that is related to the bed grain size) (Van Rijn, 1984b). Several relationships between k_s and the bed grain size have been proposed, the most widely used being $k_s = 2.5d_{50}$, when d_{50} corresponds to the median

TABLE 1 Configurations parameters.

Configuration number	U_∞ (cm/s)	d_B (cm)	Fr (-)	d_B/h (-)	u^* (cm/s)	l/h (-)
1	65	1.2	0.73	0.15	7.5	5
2	85	1.2	0.89	0.13	9.1	4.3
3	107	1.2	1.03	0.11	11.8	3.7
4	65	1.6	0.73	0.2	6.8	5
5	85	1.6	0.88	0.17	9.6	4.3
6	107	1.6	1.05	0.15	12.5	3.8
7	65	2.6	0.74	0.33	8.7	5.1
8	85	2.6	0.87	0.27	10	4.2
9	107	2.6	1.04	0.24	13.5	3.7

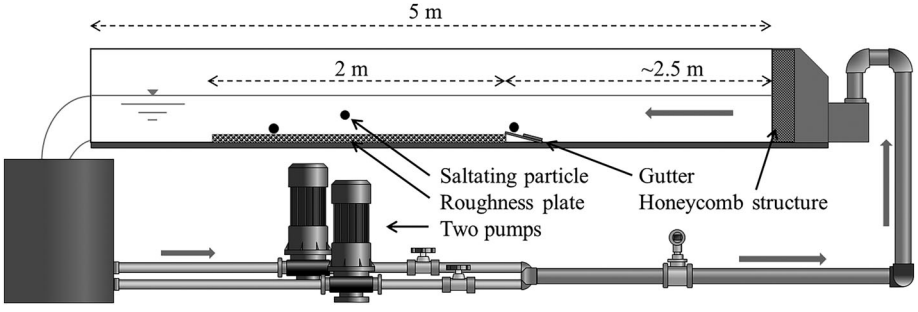

FIGURE 1 Schematic of the flume.

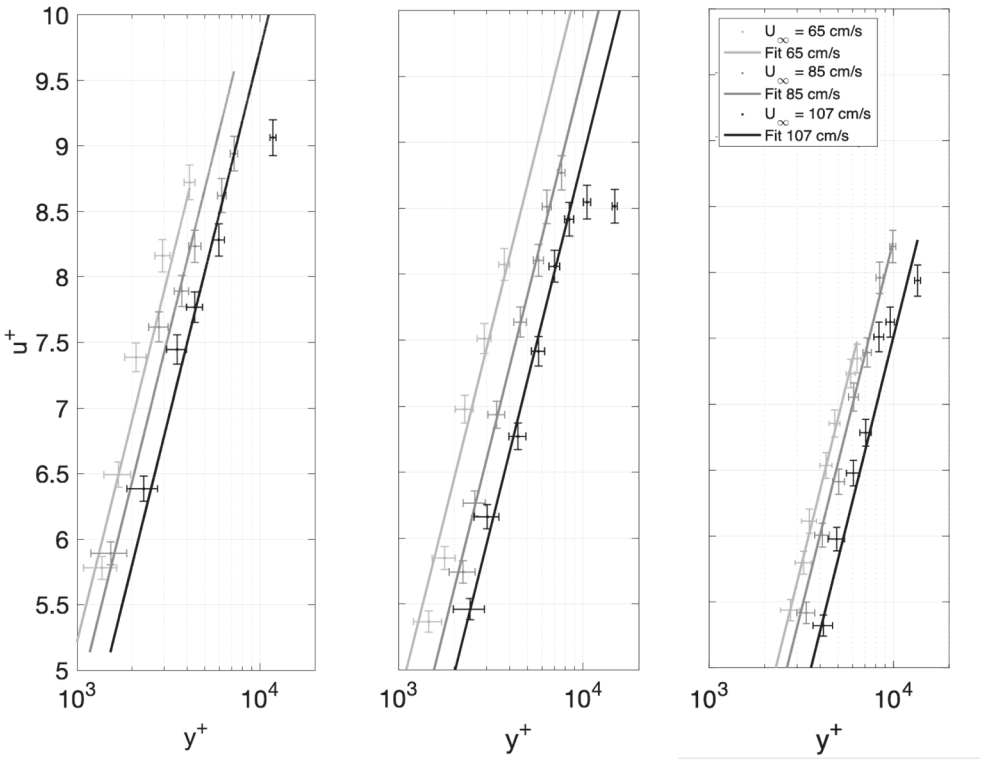

(a) $d_B = 1.2\ cm$ (b) $d_B = 1.6\ cm$ (c) $d_B = 2.6\ cm$

FIGURE 2 Flow velocity profiles and corresponding logarithmic fits for the three bed roughnesses: (a) $d_B = 1.2$ cm, (b) $d_B = 1.6$ cm and (c) $d_B = 2.6$ cm. For each roughness, three surface flow velocities were investigated 65, 85 and 107 cm/s. The horizontal and vertical axes of the graphs were non-dimensionalized using the viscous length ν/u^* and the friction velocity u^*, respectively: $y^+ = yu^*/\nu$ and $u^+ = u/u^*$. The range of regression coefficient R^2 is from 0.80 to 0.95

TABLE 2 Fall particle Reynolds number Re_p and Stokes number St for different particle diameters: $Re_p = \sqrt{gd^3(\sigma-1)/\sigma}/\nu_f$ and $St = \sigma Re_p/18$ with $\nu_f = 10^{-6}m^2/s$ and $\sigma = 2.65$ which corresponds to the density ratio between the particles and the fluid.

d (cm)	Re_p (-)	St (-)
1.6	5×10^3	7×10^2
3	1.3×10^4	1.9×10^3
5	2.7×10^4	4×10^3

diameter of the bed particles, for $d_B/h < 0.05$ (Nikuradse, 1933; Van Rijn, 1984b). y_0 depends on the universal (additive) constant in the log-law B introduced by Nikuradse (1933) ($B = (1/\kappa)\ln(k_s/y_0)$). For higher roughness-to-depth ratio, $0.05 < d_B/h < 0.25$, B decreases from 8.5 to 5 leading to y_0 multiplied by a factor of 4.2 (Czernuszenko, 2011). The parameters k_s and u^* were determined using the best logarithmic fit to the velocity measurements. The hydraulic roughness length scale is found to be proportional to the size d_B of the bed particles sizes as $k_s \approx 4.2d_B$, which is compatible with what is found in the literature (Nikuradse, 1933; Sleath, 1984; Van Rijn, 1993). The computed friction velocities are reported in Table 1.

2.3 | Experimental procedure

In order to study high Stokes number (>500), coarse particles are chosen of diameters $d = 1.6$,3 and 5 cm. Glass spheres of density ratio $\sigma = 2.65$ are used. The particles are characterized by the fall particle Reynolds number Re_p and Stokes number St, which are reported in Table 2. Particles are released one by one within the flow at the bottom of the flume towards the beginning of the rough bed section, where they experience transport as bedload, given the selected experimental conditions. The three types of particles are tested in the nine flow configurations leading to 27 different experiments. For each 27 cases, tens of particles have been released into the channel, in order to capture enough transported/saltated particles across the rough bed, so as to get representative results. The features obtained from the analysis of each individual trajectory were compiled, adding up to several hundreds of jumps for each experimental configuration.

There is a practical difficulty to introduce particles without any initial vertical or additional horizontal velocity. The following protocol has been implemented to ensure that the particles reach the rough bed with a finite horizontal velocity dependent on the flow and null initial vertical velocity. The particles have been dropped in the flow from the free surface in front of a gutter placed at the bottom of the flume (Figure 1). The gutter is made of soft material in order to absorb most of the energy of the falling particle in the gutter. It was positioned in the centre of the channel at the transition between the smooth flume bottom and the rough bed. The downstream extremity of the gutter was levelled with the rough bed. After rolling through the gutter, the particles arrived with flow horizontal velocity and no initial vertical velocity on the rough bed.

2.4 | Image analysis

The motion of the particles within a vertical plane parallel to the main flow direction is captured using a fast video camera (FastCam Photron Mini) recording 500 frames per seconds with a resolution of 1280 × 400 pixels, and that was placed looking through the side of the flume. Two led spotlights were used to illuminate the scene. The particle motion is analysed along the last metre of rough bed. The free

software Tracker (Brown, 2018) was used to extract the position of the centre of the particle on each frame (see Figure 3). A step of visual control allowing the correction of tracking errors was necessary for data quality purpose. In order to check that the transverse particle motion remains small compared with the stream-wise motion, image acquisition was first configured in down-looking view. The transverse particle motion was estimated by computing the ratio of the cross-wise to stream-wise cumulated distance travelled by the particles. The transverse motion was maximized for low speed, reaching 10% of the total stream-wise length of the observed area, indicating that the transverse motion remains marginal. Particle images were recorded travelling along the centreline of the flume throughout the field of view. In fact, the high-speed camera is focused at the centreline so that particles departing from the centreline are defocused and are eliminated automatically during image processing.

Once the particle trajectory is extracted (successive positions of particles centres), several features can be examined, starting with the height and length of the successive jumps (see Figure 3). To do so, first we identify each impact defined as a local minimum of the vertical position y of the particle and inversion of sign in the vertical velocity. The origin of y-axis is taken at the surface of the steel plate on which the bed particles are glued. If the particle is rolling, its centre never exceeds the elevation $y = d_B + d/2$ which is called in the following critical elevation y_c. Considering y_{max} as the maximum elevation between two successive impacts, illustrated Figure 3, the particle is considered into saltation if y_{max} exceeds $y_c = d_B + d/2$, representing the maximum possible vertical position of the particle touching the rough bed. With this classification of motion types, the total distances travelled through saltation or rolling motions are computed for each trajectory and expressed as per cent of the total observed length. If the particle is in saltation, the length L and the height H of the jumps are computed. L is the distance between two consecutive impacts, and H is the difference between the maximum vertical position of the particle during its jump and the vertical position at the previous impact (Berzi et al., 2016; Ishibashi, 1983). The accuracy of the height and length measurements is estimated to be within ± 0.5 mm.

In order to examine the nature of the rebound, impact and rebound velocities ($\overrightarrow{V_i}$ and $\overrightarrow{V_r}$, respectively) are computed using the particle velocities calculated from one frame before and one frame after the impact, respectively (so considering 1/500 s before and after the impact). From these velocities, rebound properties are studied in terms of the effective and vertical coefficient of restitution, e and e_y, respectively:

$$e = \frac{V_r}{V_i}, \tag{2}$$

$$e_y = \frac{V_{ry}}{V_{iy}}, \tag{3}$$

where V_i and V_r are the magnitude of the impact and rebound velocities, respectively, and V_{iy} and V_{ry} are the corresponding vertical components. The impact and rebound angle (θ_i and θ_r) can be computed as well by

$$\theta_i = \tan^{-1}\left(\frac{V_{iy}}{V_{ix}}\right), \tag{4}$$

$$\theta_r = \tan^{-1}\left(\frac{V_{ry}}{V_{rx}}\right), \tag{5}$$

where V_{ix} and V_{rx} are the horizontal components of the impact and rebound velocities, respectively.

3 | EXPERIMENTAL RESULTS

3.1 | Influence of bed roughness on saltation threshold

In our experiments, two scenarios have been identified for the motion of individual particles over the rough bed. (i) The first one, occurring in 12 out of our 27 configurations, consists in a rolling motion. The particle never detaches from the rough bed. In this case, the particle eventually stops moving after a finite time as it gets trapped in a cavity of the rough bed. (ii) In the second scenario, occurring in the remaining 15 configurations, rolling and saltation motions alternate. In this scenario, the particle keeps moving and is never trapped by the bed roughness. We can thus calculate a saltation ratio defined as the distance travelled in saltation mode to the total travelled distance. This calculation was made for each experimental configuration, combining data from individual trajectories of many particles in the same experimental conditions (coloured dots on Figure 4). The saltation ratio increases with increasing flow strength as expected. We thus have a gradual transition towards a full saltation motion. Interestingly, the saltation ratio varies as a function of bed roughness and particle diameter, indicating that these parameters play a major role in the particle motion.

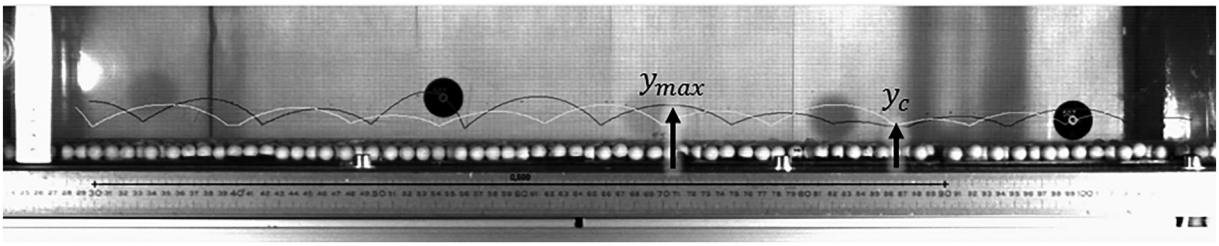

FIGURE 3 Snapshot of the video recording, with superimposed trajectories of the particles obtained from image analysis. The flow is from right to left. In this example, the bed roughness is $d_B = 1.2$ cm and the particle size is $d = 3$ cm. The trajectories of two particles (successive positions of the particles centre) are represented (black and white lines). The surface flow velocity is $U_\infty = 107$ cm/s. y_{max} corresponds to the maximum elevation between two successive impacts, illustrated for one jump along the black trajectory, $y_c = d_B + d/2$ is the maximum vertical position of the centre of a particle in rolling motion, called critical elevation, used to discriminate rolling from saltating motion.

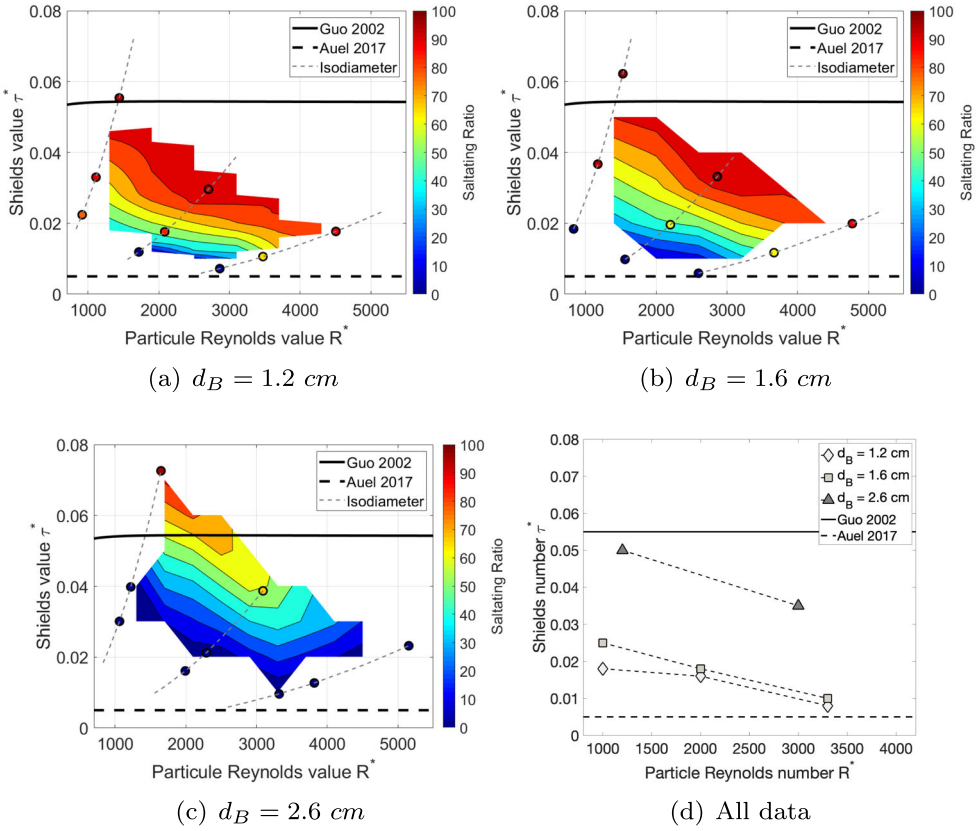

FIGURE 4 Shields diagram (τ^* vs the particle Reynolds number $R^* = du^*/\nu_f$) for the three bed roughnesses: (a) $d_B = 1.2$ cm, (b) $d_B = 1.6$ cm and (c) $d_B = 2.6$ cm. The solid and dashed lines correspond to the critical Shields value evaluated by Guo (2002) and Auel et al. (2017a), respectively. The dotted lines are the iso-diameter curves corresponding to the three particle diameters used in the experiments. The contours lines correspond to the interpolated saltation ratios. The deduced critical Shields are reported on (d).

TABLE 3 Critical Shields number and friction velocity for saltation obtained for each experimental configuration.

$d_B = 1.2$ cm			
d	1.6	3	5
d_B/d	0.75	0.40	0.24
τ_c^*	0.018	0.016	0.008
u_c^*	0.065	0.084	0.077
$d_B = 1.6$ cm			
d	1.6	3	5
d_B/d	1.00	0.53	0.32
τ_c^*	0.025	0.018	0.010
u_c^*	0.076	0.089	0.085
$d_B = 2.6$ cm			
d	1.6	3	5
d_B/d	1.62	0.87	0.52
τ_c^*	0.05	0.035	0.030
u_c^*	0.11	0.12	0.15

Note: The critical Shields number is determined for a saltation ratio of 50%.

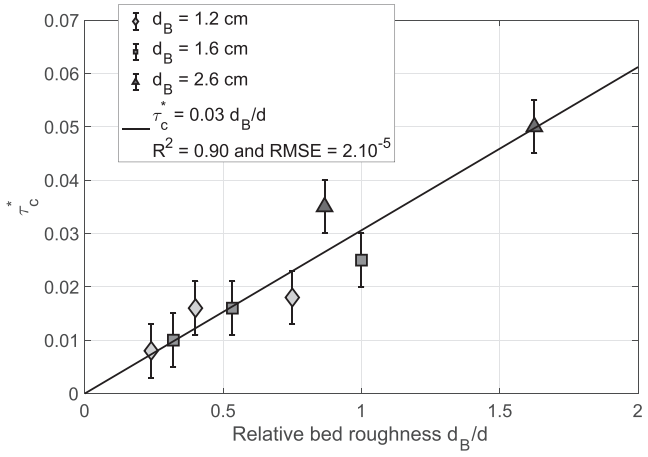

FIGURE 5 Saltation threshold τ_c^* versus relative bed roughness d_B/d.

The Shields number is defined as the dimensionless shear stress as $\tau^* = u*^2/(gd(\sigma - 1))$. Using the saltation ratio, a saltation threshold can be determined, that is, a critical Shields number corresponding to the initiation of saltation motion. The saltation threshold is here defined when the saltation ratio exceeds 50%. This is an adequate choice to allow the determination of a saltation threshold whatever the experimental conditions, because this ratio is the best represented for each roughness (Figure 4).

For a given bed roughness, a set of nine experiments is considered, combining three different particle sizes and three different flow strengths, where each of the nine experiments is characterized by a unique pair of Shields number τ^* and particle Reynolds number $R^* = du^*/\nu_f$. These values are reported in Shields diagrams (i.e., τ^* vs R^*) on Figure 4. In these diagrams, the value of the saltation ratio obtained for these nine experiments is represented with a colour code. From these information, a contour plot of isolines of saltation ratio is build using linear interpolation. The three iso-diameter lines are also plotted (dotted lines on Figure 4), each joining the points in the diagram corresponding to the same particle size used in the experiments. The saltation threshold based on 50% saltation ratio is then determined for each particle size as the intersection between the corresponding iso-diameter line and the contour line representing the 50% saltation ratio. The corresponding critical values of the

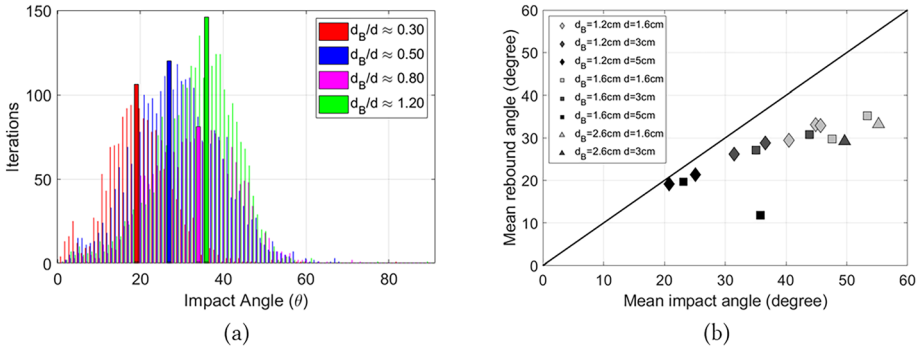

FIGURE 6 (a) Histograms of the impact angle for different values of relative bed roughness, using four approximate values of d_B/d (0.3, 0.5, 0.8 and 1.2). The principal mode is represented in bold for each relative bed roughness. (b) Mean rebound angle as a function of the mean impact angle for all experimental configurations with saltation. The solid line represents the case of a specular rebound.

Shields number are reported in Table 3. For $d_B = 1.2$ cm, these values ranges from 0.008 to 0.02, for $d_B = 1.6$ cm from 0.01 to 0.025 and for $d_B = 2.6$ cm from 0.03 to 0.05.

Introducing the relative bed roughness defined as d_B/d (our set of experimental configurations comprises nine values of relative bed roughness, see Table 3), the saltation threshold varies almost linearly with the relative bed roughness d_B/d as illustrated in Figure 5:

$$\tau_c^* \approx \tau_{c0}^* \frac{d_B}{d}, \tag{6}$$

with $\tau_{c0}^* \approx 0.03$ representing the critical Shield number for $d_B = d$. This scaling combines the effects of bed roughness and particle size to provide a good approximation of the saltation threshold.

3.2 | Influence of bed roughness on impact

Saltation depends crucially on the characteristics of the particle impact. It is then essential to investigate the role of the bed roughness on the impact. First, we focus on the statistical distribution of the impact angle θ_i as a function of the relative bed roughness (see Figure 6a). Each of the 15 experimental configurations where saltation is observed includes more than 400 jumps except for the case where $d = 5$ cm, $d_B = 1.2$ cm and $U_\infty = 107$ cm/s for which only 115 jumps have been recorded. In order to have a regular distribution of d_B/d, and to have a similar number of jumps in each, we gather the jumps using four approximate values of d_B/d: 0.3, 0.5, 0.8 and 1.2. We note a systematic shift of the distributions towards high angles for increasing relative bed roughness. The main mode, the mean and the median values are reported in Table 4. All three values increase with increasing bed roughness. Similarly, on Figure 6b, the mean rebound angle increases as the mean impact angle is increased. Large relative bed roughness thus favours large impact and rebound angles in contrast with small roughness. Interestingly, the rebound is not specular: The rebound angle is always smaller than the impact angle. This is a generic feature for rebound on a rough bed (Beladjine et al., 2007). A second minor mode θ_{mod2} is detected for each bed roughness showing small impact angle about 5° quasi-independent on the bed roughness. This second mode represents about 10% of the jumps.

Going a step further in the analysis of the impact, we characterize the loss of energy in the collision process by examining both coefficients of restitution e and e_y (Figure 7), usually employed in the literature to describe the collision. Experimental and numerical studies on the collision process of an incident particle onto a granular bed made

TABLE 4 Impact angle as a function of the relative bed roughness d_B/d.

	$d_b/d \approx 0.30$	$d_b/d \approx 0.50$	$d_b/d \approx 0.80$	$d_b/d \approx 1.20$
θ_{mod1}	19.0°	27.0°	34.0°	36.0°
θ_{mod2}	3.8°	5.4°	5.8°	6.0°
θ_{mean}	19.5°	28.3°	32.0°	32.6°
θ_{median}	19.0°	28.0°	32.3°	33.5°

of similar particles reported that the effective restitution coefficients exhibit a dependence with the impact angle (Beladjine et al., 2007), which can be approximated by

$$e = A - B\sin\theta_i, \tag{7}$$

$$e_y = A_y/\sin\theta_i - B_y, \tag{8}$$

where A, B, A_y and B_y are constant parameters that depend on the material properties of the particle and the bed. In the experimental work of Beladjine et al. (2007) where they used PVC particles of similar size for the bed and the incident particle, they reported the following values for the aforementioned parameters: $A = 0.87, B = 0.72, A_y = 0.30$ and $B_y = 0.15$.

Concerning the restitution coefficient e, the data collapse on a single curve (see Figure 7a), without showing a noticeable dependence on the relative bed roughness. The coefficient of restitution e exhibits a weak decrease with the impact angle as expected from the previous studies. The tendency matches the law Equation (7) with $A = 1$ and $B = 0.26, A$ being 1 is in agreement with Gondret et al. (2002) for glass spheres with negligible lubrication effects. Nevertheless, the data are scattered for impact angles superior to 45°, due to too few jumps exhibiting such angles, preventing us to conclude for this range of values. In contrast, the relative bed roughness has a clear effect on the restitution coefficient e_y (see Figure 7b). The higher the relative bed roughness, the higher the vertical restitution coefficient. Around a given value of relative bed roughness, the vertical restitution e_y is a decreasing function of the impact angle, well approximated by the inverse function in Equation (8). The fit parameters A_y and B_y are reported in Table 5. A_y increases with bed roughness demonstrating a more efficient transfer of energy to vertical momentum for higher roughness. Nevertheless, as for the restitution coefficient, the range above 45° is poorly represented. Interestingly, the vertical restitution coefficient reaches very high values at grazing impact angle, greater than one, reaching 4 for angles between 5° and 10°. This result shows that for low impact angle, there is an efficient conversion of the

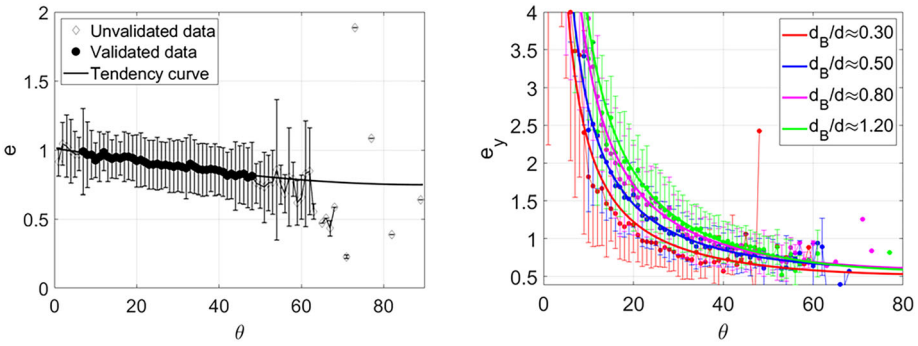

FIGURE 7 (a) Restitution coefficient e versus θ_i. The solid line is the best fit to the data according to the following law: $e = A - B\sin\theta_i$ with $A = 1.01$ and $B = 0.26$. (b) Restitution coefficient e_y versus the angle of impact according to the four approximate values of relative bed roughness. The solid lines are the best fits to the data according to the following law: $e_y = A_y/\sin\theta_i - B_y$ with the coefficients given in Table 5. On both figures, error bars are provided for each subset of collisions as the data were binned at 1°.

TABLE 5 Coefficient A_y and B_y appearing in Equation (8).

	$d_b/d \approx 0.30$	$d_b/d \approx 0.50$	$d_b/d \approx 0.80$	$d_b/d \approx 1.20$
A_y	0.36	0.45	0.58	0.68
B_y	0.16	0.15	0.03	−0.10

horizontal momentum of the incident particle into vertical momentum of the particle after collision. The second mode of impact angle, showing could thus play a key role in extremely high jumps compared with the averaged jumps. All these results highlight the importance of the relative bed roughness and the impact angle on the properties of the rebound: Bed roughness, by increasing the vertical restitution, increases the height of the trajectory, influencing the trajectory of the particles.

3.3 | Distribution of jump length and height

Figure 8 shows typical distributions of jump height and length obtained (here, for $d = 3$ cm particles on $d_B = 1.2$ cm rough bed for a flow surface velocity $U_\infty = 107$ cm/s and comprising 1181 recorded jumps). First, the distributions of the jump height and length exhibit a single mode but are not symmetric. The modal value is different from the mean value. The jump height distribution can be well represented by a log-normal distribution while the jump length is closer to a Gamma distribution, as shown in Figure 8. This is in agreement with the literature and confirms the reliability of the statistics.

From these distributions, mean and standard deviation of the jump height and length can be computed. They are reported in Tables 6 and 7. The mean height $\overline{H}$ and length $\overline{L}$ increase with increasing flow strength and bed roughness. This will be examined in further details in the next subsection. The standard deviation of jump length is between 20% and 50% of the mean jump length while the standard deviation of jump height is in general greater than 50% of the mean jump height.

3.4 | Variation of the mean jump height and length with the flow strength and bed roughness

Sklar and Dietrich (2004) and Auel et al. (2017a) reported many experimental results under various experimental conditions (bed slope ranging from 0 to 0.40, mobile or fixed beds with particle diameter ranging from 0.5 to 31 mm and shear velocity ranging from 0.01 to 0.23 m/s). They established general formulas for the mean jump height and length in terms of the relative excess shear stress $T = \tau^*/\tau_c^* - 1$ where τ_c^* is the critical Shields for incipient motion. They found that the jump height and length rescaled by the particle diameter obey a scaling law as a function of the relative excess shear stress:

$$\frac{\overline{H}}{d} = a_H T^{\chi_H}, \tag{9}$$

$$\frac{\overline{L}}{d} = a_L T^{\chi_L}. \tag{10}$$

The parameters a_H and a_L and the exponents (χ_H and χ_L) are obtained from a fit to the experimental data. Sklar and Dietrich (2004) and Auel et al. (2017a) obtained rather different values: $a_H \approx 1.44, \chi_H \approx 0.5, a_L \approx 8$ and $\chi_L \approx 0.88$ for Sklar and Dietrich (2004) and $a_H \approx 0.7, \chi_H \approx 0.3$, $a_L \approx 2.3$ and $\chi_L \approx 0.8$ for Auel et al. (2017a). The significant difference between these two experimental studies as well as the scattering of the measured data certainly means that an important parameter is missing in this formula.

In order to compare our results with the previous published dataset, we consider no slope, high Stokes datasets (Auel et al., 2017a; Niño et al., 1994) and dataset investigating different values of bed roughness (Bhattacharyya et al., 2013; Hu & Hui, 1996; Lee & Hsu, 1994). Details of these datasets are compiled in Table 8. As the bed roughness is expected to play an important role in the characteristics of the particle trajectories, we introduce explicitly in the scaling laws the dependence on the relative roughness and obtain

$$\frac{\overline{H}}{d} = (d_B/d)^{1.75} T^{0.75}. \tag{11}$$

And

$$\frac{\overline{L}}{d} = 5(d_B/d)^{1.15} T^{0.75}. \tag{12}$$

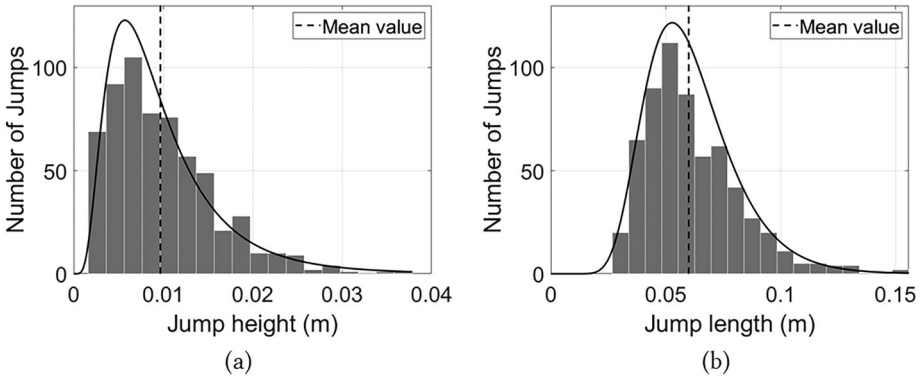

FIGURE 8 Distributions of jump (a) height H and (b) length L obtained for d3 cm particles on d_B1.2 cm rough bed for a flow surface velocity $U_\infty = 107$ cm/s. The continuous curves correspond to a log-normal distribution for (a) H and to a Gamma distribution for (b) L. The dashed lines correspond to the mean values $\overline{H}$ and $\overline{L}$.

TABLE 6 Mean jump height and associated standard deviation for each experimental configuration.

	65	85	107	65	85	107
Velocity of the flow (cm/s)	$\overline{H}$ (cm)			Standard deviation (cm)		
$d_B = 1.2$ cm						
$d = 1.6$ cm	0.3	1.1	1.3	0.2	0.6	0.8
$d = 3$ cm	-	0.5	1.1	-	0.3	1.0
$d = 5$ cm	-	0.3	0.6	-	0.2	0.45
$d_B = 1.6$ cm						
$d = 1.6$ cm	-	1.3	2.0	-	0.7	1.1
$d = 3$ cm	-	0.4	1.0	-	0.2	0.6
$d = 5$ cm	-	0.2	0.5	-	0.1	0.3
$d_B = 2.6$ cm						
$d = 1.6$ cm	-	-	1.8	-	-	0.9
$d = 3$ cm	-	-	0.6	-	-	0.3
$d = 5$ cm	-	-	-	-	-	-

Note: The cases with no data correspond to the rolling regime.

TABLE 7 Mean jump length and associated standard deviation for each experimental configuration.

	65	85	107	65	85	107
Velocity of the flow (cm/s)	$\overline{L}$ (cm)			Standard deviation (cm)		
$d_B = 1.2$ cm						
$d = 1.6$ cm	1.3	4.8	7.0	0.8	1.8	2.8
$d = 3$ cm	-	2.6	7.0	-	1.0	3.8
$d = 5$ cm	-	2.9	6.4	-	0.9	1.9
$d_B = 1.6$ cm						
$d = 1.6$ cm	-	4.5	9.6	-	2.0	3.6
$d = 3$ cm	-	1.7	6.0	-	1.1	2.1
$d = 5$ cm	-	1.7	4.5	-	0.4	1.52
$d_B = 2.6$ cm						
$d = 1.6$ cm	-	-	6.7	-	-	3.3
$d = 3$ cm	-	-	2.5	-	-	1.6
$d = 5$ cm	-	-	-	-	-	-

Note: The cases with no data correspond to the rolling regime.

Doing so, the data for the mean jump height and length collapse on a unique law independent of the bed roughness and particle size (see Figure 9) except for (Auel et al., 2017a) dataset that is aligned with the others but separated. The influence of the bed roughness is encoded through both the relative roughness and the saltation threshold τ_c^* (which depends on the bed roughness as seen in Equation 6). Auel et al. (2017a) conducted experiments with a fixed bed made of mortar and found a critical Shields number of 0.005. Our correlation law (see Equation 6) gives a critical value of 0.005 for a relative bed roughness of 0.16. Although this makes it difficult to evaluate the roughness of mortar bed, 0.16 would give a roughness of about 0.1 mm which could act as a minimal value of bed roughness, leading to consider 0.005 as the minimal threshold. Chatanantavet et al. (2013) obtained as well a critical value of 0.007 for mortar. Besides, the critical values reported in the literature concern the threshold for incipient motion which may differ slightly from the saltation threshold defined here. This may explain the discrepancy observed on Figure 9.

Combining the scaling laws for non-dimensionalized $\overline{H}$ and $\overline{L}$ (Equations 11 and 12), the trajectory index $\overline{L}/\overline{H}$, the jump length-to-jump height ratio (inverse of the aspect ratio), is shown independent of the flow strength (which is different to what was found in Auel et al., 2017a; Sklar & Dietrich, 2004) but depends on the relative bed roughness. Actually, this is particularly true for experiments with $St > 500$ (Auel et al., 2017a; Niño et al., 1994), as shown in Figure 10: The trajectory index decreases with increasing roughness. Nonetheless, Figure 10 shows that for St from 200 to 500 (Auel et al., 2017a), for small relative roughness (e.g., $d_B/d < 0.2$, corresponding to mortar), shear still plays a role, whereas for d_B/d about 1, the shear has less influence on the trajectory index. For a given relative bed roughness d_B/d, our data indicate that the jump length varies linearly with the jump height with a factor close to 5. In our set of experiments, the highest observed length-to-height ratio is about 10 for the lowest relative bed roughness (i.e., $d_B/d \approx 0.3$) whereas the length-to-height ratio falls to about 4 for the largest relative bed roughness (i.e., $d_B/d \approx 1.2$). These experimental outcomes confirm the crucial role of the bed roughness on the features of the particle trajectories.

4 | DISCUSSION

In marine environment with extreme tidal current, large particles are put into motion, on beds constituted of different sizes. Such motion is characterized by high Stokes number ($St > 500$). Although some previous studies have considered several roughnesses, the differences with prior work lies in the large range of relative bed roughness d_B/d, which varies from 0.24 to 1.62 in our experiments, and a large Stokes and particle Reynolds numbers considered, up to 4000 and 5000,

TABLE 8 Comparison with the literature.

References	d_B (mm)	d (mm)	d_B/d (-)	Shields $\times 10^{-2}$	St (-)	Shape
Lee and Hsu (1994)	1.36	1.36–2.5	0.5–1	6–46	7–21	Spherical
Bhattacharyya et al. (2013)	1–2	1–2	0.5–2	1.5–6	11–33	Spherical
Hu and Hui (1996)	1.36–7.6	2–4	~2	7–140	3–56	Natural
Auel et al. (2017a)	$ks = 0.2$	5.3–18.5	0.01–0.04	8–64	44–585	Spherical
Niño et al. (1994)	15–31	15–31	1	9–14	1090–3200	Natural
Present study	12–26	16–50	0.5–1.625	1–7	560–4000	Spherical

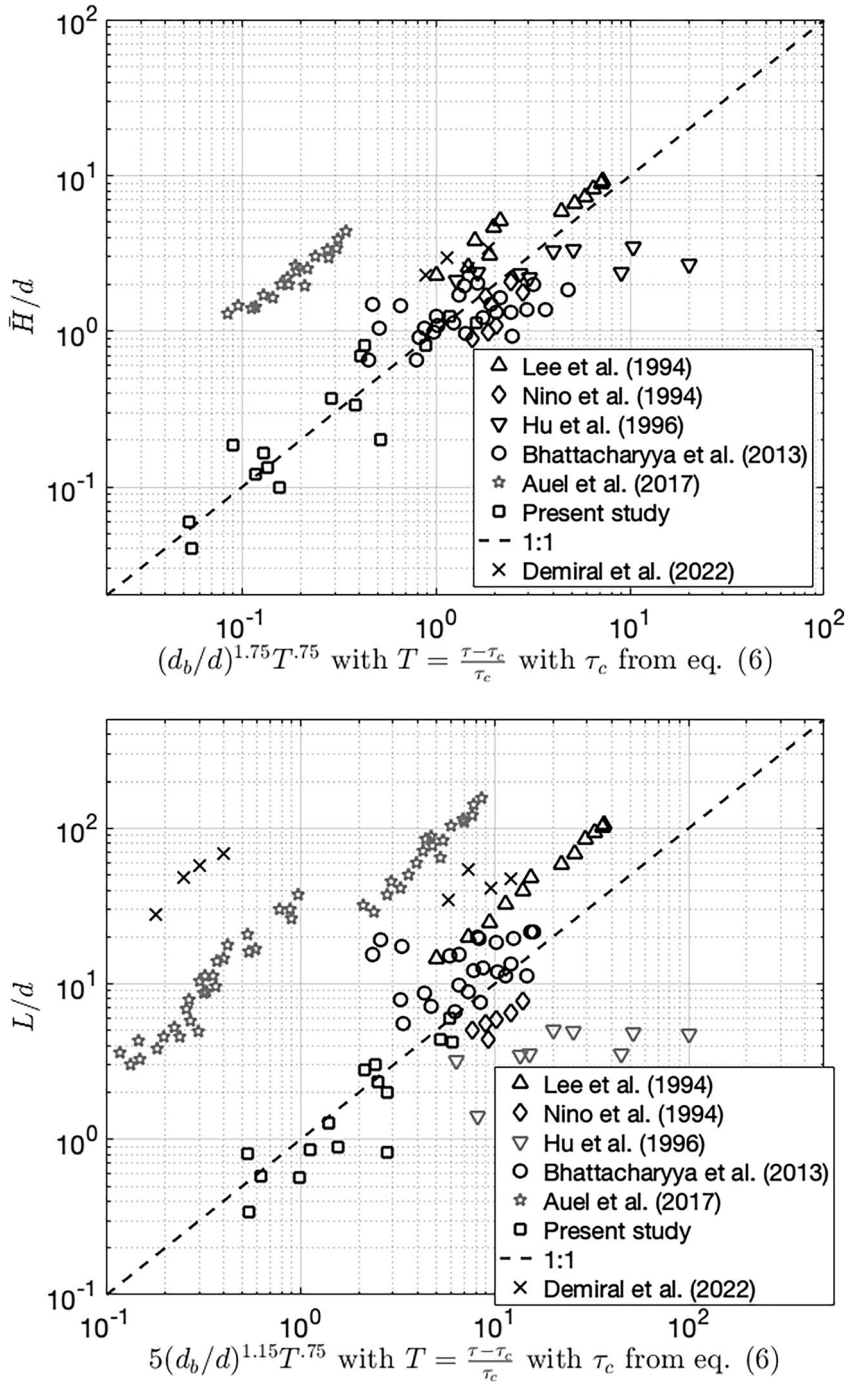

FIGURE 9 Dimensionless mean jump height $\overline{H}/d$ (*top*) and dimensionless mean jump length $\overline{H}/d$ (*bottom*) as a function of the relative excess shear stress $T = (\tau^* - \tau_c^*)/\tau_c^*$ and the relative roughness d_B/d. The scaling law are, respectively, $\overline{H}/d \approx (d_B/d)^{1.75}T^{0.75}$ and $\overline{L}/d \approx 5(d_B/d)^{1.15}T^{0.75}$.

respectively. So our study deals with the influence of bed roughness in such conditions. At the scale of individual jumps, the mean impact angle is shown closely related to the bed roughness: An increase of the relative bed roughness leads to an increase of the mean impact angle (from 19.5° to 32.6° for $d_B/d = 0.3$ and 1.20, respectively). This is in agreement with previous work by Niño et al. (1994) and Demiral

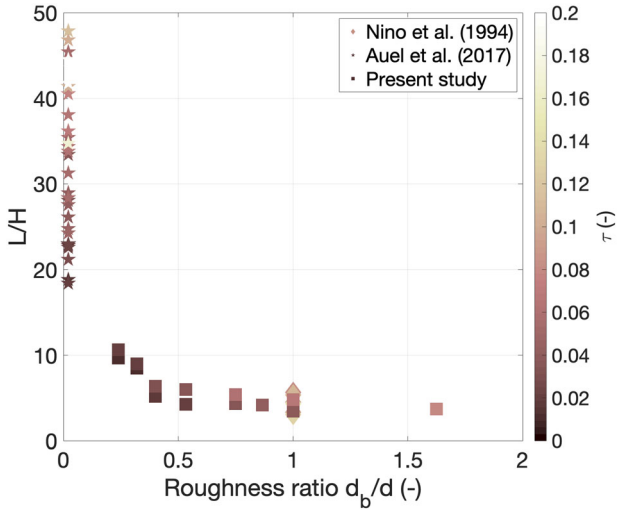

FIGURE 10 Length-to-height ratio $\overline{L}/\overline{H}$ as a function of the relative bed roughness d_B/d coloured by the dimensionless shear τ for data exhibiting high Stokes number ($St > 500$).

et al. (2022). This result can be explained with the characteristics of the rebound, which reveal two key features. First, for a given bed roughness, the vertical restitution coefficient (which is the ratio of the vertical rebound velocity and the vertical impact velocity) is a decreasing function of the impact angle and reaches values greater than 1 for grazing impacts, as observed in aeolian saltation transport (Beladjine et al., 2007; Berzi et al., 2016). In order to sustain saltation motion, the vertical restitution coefficient needs to be slightly greater than 1 to compensate for viscous dissipation during the ascent of the particle. According to Figure 7b, this means that the impact angle should be inferior to 25°, 30°, 37° and 38° for relative roughness of 0.3, 0.5, 0.8 and 1.2, respectively. The first mode reported for each of our configuration is slightly smaller than these values (19°, 27°, 34° and 36° from Table 4) which is in agreement with a sustainable saltation transport. It is interesting to note that a second minor mode (second maximum in the impact angle distribution) is observed for grazing impact angles (about 5° whatever the bed roughness). Because for such grazing angles, the vertical restitution coefficient is about 4, this would lead to quasi-vertical trajectory. This is in agreement with regular occurrence of quasi-vertical trajectories. However, for small values of impact angles, not enough occurrence are recorded leading to an important scattering. The precise modal value of this second mode should be determined with more trials/jumps. Nevertheless, the existence of this minor mode has also been noticed by Valance and Berzi (2022) in numerical modelling. Second, for a given impact angle, the vertical restitution coefficient is found to increase with increasing bed roughness. As a result, the optimum impact angle for sustained saltation is increased as the bed roughness increases, as observed in our experiments. This demonstrates the key role of the collision process, as emphasized by Tsuchiya (1969), and consequently of the bed roughness, in the saltation motion and as a consequences in the particle trajectory. Besides, Auel et al. (2017b) shown that for fixed planar beds, the impact angle is about 4° and is almost equivalent to the rebound angle, with a vertical restitution coefficient superior to one, up to 5. Niño et al. (1994) on rough bed with a roughness ratio of one and Stokes number in the range [1090–3200] obtained impact angle about 18° and rebound angle bigger (about 30°) but with a standard deviation of more than 50%. This latter obtained vertical restitution coefficient less than 0.5, suggesting a motion that is not sustainable. Our results show impact angle up to 40°, depending on the bed roughness. The rebound angle is similar to the impact angle up to 30° and becomes smaller and smaller with increasing relative bed roughness. This would lead to trajectory inverted to what is commonly found in the literature. Nevertheless, for such high angles, the vertical restitution coefficient is below one, leading to non-sustainable saltation. Moreover, our data are more scattered in this part. The flow strength does not seem to have an impact on the impact angle nor on the restitution coefficient in agreement with Niño et al. (1994) and Auel et al. (2017b). Our results confirm that the jump height and length increase with increasing flow strength (Abbott & Francis, 1977; Auel et al., 2017a; Chatanantavet et al.2013; Demiral et al., 2022). They also show significant changes in the characteristics of the particle trajectories according to the relative bed roughness. This differs significantly from other studies with similar particle diameters and flows strengths (Auel et al., 2017a; Ishibashi, 1983; Niño et al., 1994). Interestingly, our data indicate that both the jump height and length increase with increasing bed roughness, in agreement with the results of Bhattacharyya et al. (2013). However, in contrast with the latter study where they found that the trajectory index L/H is almost invariant with the bed roughness, our results for $St > 500$ (Figure 10) reveal that it decreases significantly with the relative roughness d_B/d (from 11 to 4). Considering that the range of relative bed roughnesses is almost the same in both studies, these differences may be explained by the fact that our experimental conditions lie in the regime of high Stokes numbers with particles of several centimetres (thus, one order of magnitude bigger than Bhattacharyya et al., 2013) where the role of viscous dissipation in collisions is expected to be marginal. In contrast, the experiments of Bhattacharyya et al. (2013) were conducted with smaller particles (from 1 to 2 mm), thus in a regime of much lower Stokes number ($St \sim 30$). Compared with experiments with Stokes number >500 (Figure 10) (Auel et al., 2017a; Niño et al., 1994), the trajectory index is comparable with our results and the shear is shown to have few influence as the relative bed roughness becomes closer to one.

Our experimental results reveal that the critical Shields number for saltation increases with increasing relative bed roughness d_B/d where d_B is the diameter of the particle from the rough bed and d is the size of the saltating particle (Equation 6). This was also reported by Demiral et al. (2022). For the smallest relative bed roughness (i.e., $d_B = 0.24d$) we get a critical Shields number of 0.008 while for the largest one (i.e., $d_B = 1.62d$), we obtain a value of 0.05. In the range of particle Reynolds number R^* corresponding to our experiments (from 1000 to 5000), the critical Shields number for incipient motion according to the Shields curve is constant and is about 0.05 (Guo, 2002; Shields, 1936) for a mobile bed for d_B/d close to one. On a fixed bed, as in our experiments, Abbott and Francis (1977) find a critical value of 0.03 with a relative bed roughness d_B/d close to 1, in agreement with the relationship we propose. 0.005 is fixed as minimal threshold, being associated to the critical Shields over mortar (Auel et al., 2017a; Chatanantavet et al., 2013). This threshold is for saltation. The influence of secondary currents remains unclear here. Albayrak and Lemmin (2011) have investigated the presence of secondary currents for width-to-depth ratio about 20, demonstrating the presence of many vertical secondary currents that could enhance or

not the trajectory. Even if the variations of the current remains less than 5% of the main stream in the channel, it could influence the trajectory. However, the number of jumps studied over a wide range of horizontal positions, in the middle of the channel lead certainly to avoid its influence. According to Demiral et al. (2022), as bed roughness increases, secondary currents become more pronounced and result in higher particle acceleration rates near the bed and thus higher jumps.

Importantly, we also find than the jump height and length obey a unique power law with the excess shear $(\tau^* - \tau_c^*)/\tau_c^*$ using Equation (6) for τ_c^* and scaled by a power of relative roughness, leading to a trajectory index independent of the shear stress. This is notably demonstrated for data with high Stokes number and relative roughness close to one. This result differs from previous studies (Auel et al., 2017a; Sklar & Dietrich, 2004), that does not consider bed roughness in their scaling, leading to a scattering of the data of several order of magnitudes with their power laws. Our proposed laws clearly improved the prediction of the jumps parameters in inertial regime ($St > 500$).

5 | CONCLUSION

Our study deals with saltation in the inertial regime (i.e., large Stokes number) over fixed beds with various roughnesses. By varying the bed roughness over a large range, we show that it has a major impact on the saltation motion and threshold. The vertical restitution coefficient is shown to increase with bed roughness, leading to higher jumps. Considering that an optimal angle is found for a vertical restitution about one (required to sustain saltation motion), this leads to higher optimum angles for higher roughness-to-particle ratio. A second minor mode is observed for grazing impact angles (about 5° whatever the bed roughness) leading to quasi-vertical trajectories, coherent with our observations. This minor mode could actually be the one responsible for turbines damages, 1 m above bottom, in megatidal environment and would necessitate more investigations. The initiation of the motion is shown to depend on the bed roughness as well, and this is confirmed by the different values found in the literature. Power laws of the excess shear stress are proposed for jump height and length, taking into account the bed roughness. They are shown reliable with dataset from the literature. The new definition of the critical Shields number, varying with bed roughness, is taken into account in the proposed relationships, even if it is shown to have minor influence on the reliability of the proposed laws. For high Stokes number, in inertial regime, the bed roughness has more influence on the collision process and the trajectory of the particles than for non-inertial motion where viscous forces play a key role. Jump height and length increase with bed roughness, with height increasing quicker than length leading to a more vertical trajectory for higher bed roughness. This is an issue when envisioning to put hydrokinetic turbines in environment experiencing coarse particle saltation. Lastly, the experimental outcomes presented here constitute a good basis for testing models and simulations. As showed above, the boundary conditions at the bed play a major role in the particle motion, and we provide here a full description of the impact process, which is a key ingredient for developing quantitative models for particle transport.

AUTHOR CONTRIBUTIONS

We confirm that the manuscript has been read and approved by all named authors and that there are no other persons who satisfied the criteria for authorship but are not listed. We further confirm that the order of authors listed in the manuscript has been approved by all of us.

ACKNOWLEDGEMENTS

The work was supported by Agence Nationale de la Recherche FEM project PHYSIC (ANR-10-IEED-0006-10) and by ISblue project, Interdisciplinary graduate school for the blue planet (ANR-17-EURE-0015) and co-funded by a grant from the French government under the programme 'Investissements d'Avenir' embedded in France 2030. We confirm that we have given due consideration to the protection of intellectual property associated with this work and that there are no impediments to publication, including the timing of publication, with respect to intellectual property. In so doing, we confirm that we have followed the regulations of our institutions concerning intellectual property.

CONFLICT OF INTEREST STATEMENT

We wish to confirm that there are no actual or potential conflict of interest including any financial, personal or other relationships with other people or organizations within 3 years of beginning the submitted work that could inappropriately influence, or be perceived to influence, the present work.

DATA AVAILABILITY STATEMENT

The dataset is available and has a DOI (https://doi.org/10.5281/zenodo.7674868).

ORCID

France Floc'h https://orcid.org/0000-0001-9643-2278

REFERENCES

Abbott, J.E. & Francis, J.R.D. (1977) Saltation and suspension trajectories of solid grains in a water stream. *Philosophical Transactions of the Royal society of London*, 284(1321), 225–254.

Albayrak, I. & Lemmin, U. (2011) Secondary currents and corresponding surface velocity patterns in a turbulent open-channel flow over a rough bed. *Journal of Hydraulic Engineering*, 137(11), 1318–1334.

Ancey, C., Bigillon, F., Frey, P., Lanier, J. & Ducret, R. (2002) Saltating motion of a bead in a rapid water stream. *Physical Review E—Statistical, Nonlinear, and Soft Matter Physics*, 66(3), 1–16.

Auel, C., Albayrak, I., Sumi, T. & Boes, R.M. (2017a) Sediment transport in high-speed flows over a fixed bed: 1. Particle dynamics. *Earth Surface Processes and Landforms*, 42(9), 1365–1383.

Auel, C., Albayrak, I., Sumi, T. & Boes, R.M. (2017b) Sediment transport in high-speed flows over a fixed bed: 2. Particle impacts and abrasion prediction. *Earth Surface Processes and Landforms*, 42(9), 1384–1396.

Beladjine, D., Ammi, M., Oger, L. & Valance, A. (2007) Collision process between an incident bead and a three-dimensional granular packing. *Physical Review E—Statistical, Nonlinear, and Soft Matter Physics*, 75(6), 1–12.

Berzi, D., Jenkins, J.T. & Valance, A. (2016) Periodic saltation over hydrodynamically rough beds: aeolian to aquatic. *Journal of Fluid Mechanics*, 786, 190–209.

Bhattacharyya, A., Ojha, S.P. & Mazumder, B.S. (2013) Evaluation of the saltation process of bed materials by video imaging under altered bed roughness. *Earth Surface Processes and Landforms*, 38(12), 1339–1353.

Blanpain, O. (2009) Dynamique 'dimentaire Multiclasse: De l'tude des processus la mod'lisation en Manche. Ph.D. Thesis, Université de Bretagne Occidentale.
Brown, D. (2018) Tracker: video analysis and modeling tool.
Buffington, J.M., Dietrich, W.E. & Kirchner, J.W. (1992) Friction angle measurements in a naturally formed gravel streambed: implications for critical boundary shear stress. *Water Resources Research*, 28(2), 411–425.
Cada, G., Ahlgrimm, J., Bahleda, M., Bigford, T., Stavrakas, S.D., Hall, D., Moursund, R. & Sale, M. (2007) Potential impacts of hydrokinetic and wave energy conversion technologies on aquatic environments. *Fisheries*, 32(4), 174–181.
Chatanantavet, P. (2007) Physically-based models of bedrock incision processes in mountain streams. Ph.D. Thesis, University of Minnesota.
Chatanantavet, P., Whipple, K.X., Adams, M.A. & Lamb, M.P. (2013) Experimental study on coarse grain saltation dynamics in bedrock channels. *Journal of Geophysical Research: Earth Surface*, 118(2), 1161–1176.
Czernuszenko, W. (2011) Spatially averaged log-law for flows over rough bed in zero-and non-zero-pressure gradient boundary layers. *Archives of Hydro-Engineering and Environmental Mechanics*, 58(1-4), 65–86.
Dancey, C.L., Diplas, P., Papanicolaou, A. & Bala, M. (2002) Probability of individual grain movement and threshold condition. *Journal of Hydraulic Engineering*, 128(12), 1069–1075.
Delannay, R., Valance, A., Mangeney, A., Roche, O. & Richard, P. (2017) Granular and particle-laden flows: from laboratory experiments to field observations. *Journal of Physics D: Applied Physics*, 50(5), 53001.
Demiral, D., Albayrak, I., Turowski, J.M. & Boes, R.M. (2022) Particle saltation trajectories in supercritical open channel flows: roughness effect. *Earth Surface Processes and Landforms*, 47(15), 3588–3610.
Dey, S. (2003) Threshold of sediment motion on combined transverse and longitudinal sloping beds. *Journal of Hydraulic Research*, 41(4), 405–415.
Fernandez Luque, R. & Van Beek, R. (1976) Erosion and transport of bedload sediment. *Journal of Hydraulic Research*, 14(2), 127–144.
Francis, J.R.D. (1973) Experiments on the motion of solitary grains along the bed of a water-stream. *Proceedings of the Royal Society A: Mathematical, Physical and Engineering Sciences*, 332(1591), 443–471.
Gessler, J. (1970) Self-stabilizing tendencies of alluvial channels. *Journal of the Waterways, Harbors and Coastal Engineering Division*, 96(2), 235–249.
Gilbert, G.K. & Murphy, E.C. (1914) *The transportation of debris by running water*. Washington: US Government Printing Office.
Gondret, P., Lance, M. & Petit, L. (2002) Bouncing motion of spherical particles in fluids. *Physics of Fluids*, 14(2), 643–652.
Guo, J. (2002) Hunter Rouse and Shields diagram. *Advances in Hydraulics and Water Engineering* I and II: 1096–1098.
Hu, C. & Hui, Y. (1996) Bed-load transport. I: mechanical characteristics. *Journal of Hydraulic Engineering*, 122(5), 245–254.
Ishibashi, T. (1983) A hydraulic study on protection for erosion of sediment flush equipments of dams, Proceedings of the Japan Society of Civil Engineers, Japan Society of Civil Engineers.
Joseph, D.D. & Hunt, M.L. (2004) Oblique particle-wall collisions in a liquid. *Journal of Fluid Mechanics*, 510(2004), 71–93.
Lajeunesse, E., Malverti, L. & Charru, F. (2010) Bed load transport in turbulent flow at the grain scale: experiments and modeling. *Geophysical Research Earth Surface*, 115, F04001.
Lee, H.Y. & Hsu, I.S. (1994) Investigation of saltating particle motions. *Journal of Hydraulic Engineering*, 120(7), 831–845.
Neill, C.R. & Yalin, M.S. (1969) Quantitative definition of beginning of bed movement. *Journal of the Hydraulics Division*, 95(1), 585–588.
Niño, Y. & Garcìa, M. (1998) Using Lagrangian particle saltation observations for bedload sediment transport modelling. *Hydrological Processes*, 12(8), 1197–1218.
Niño, Y., García, M. & Ayala, L. (1994) Gravel saltation: 1. Experiments. *Water Resources Research*, 30(6), 1907–1914.
Nikuradse, J. (1933) Stramungsgestze in rauhen rohren. *Ver. Deut. Ing.*, 361, 1.
Papanicolaou, A.N., Diplas, P., Evaggelopoulos, N. & Fotopoulos, S. (2002) Stochastic incipient motion criterion for spheres under various bed packing conditions. *Journal of Hydraulic Engineering*, 128(4), 369–380.
Rahim, A. & Stevens, R.F. (2013) Design procedures for marine renewable energy foundations, Proceedings of the 1st Marine Energy Technology Symposium: METS 2013, April. Washington, DC.
Ramesh, B., Kothyari, U.C. & Murugesan, K. (2011) Near-bed particle motion over transitionally-rough bed. *Journal of Hydraulic Research*, 49(6), 757–765.
Rouse, H. (1939) *Experiments on the mechanics of sediment suspension*. Fifth International congress for applied mechanics. Cambridge, MA: John Wiley & Sons.
Sekine, M. & Kikkawa, H. (1992) Mechanics of saltating grains. II. *Journal of Hydraulic Engineering*, 118(4), 536–558.
Shields, A. (1936) *Application of similarity principles and turbulence research to bed-load movement*. Pasadena: California Institute of Technology.
Sklar, L.S. & Dietrich, W.E. (2004) A mechanistic model for river incision into bedrock by saltating bed load. *Water Resources Research*, 40(6), 1–22.
Sleath, J.F.A. (1984) *Sea bed mechanics*. John Wiley & Sons Inc.: New York, NY.
Tsuchiya, Y. (1969) On the mechanics of the successive saltation of a sand particle on a granular bed in a turbulent stream. *Proceedings of the 13th Congress, IAHR*, 2, 191–198.
Valance, A. & Berzi, D. (2022) Particle saltation over rigid bumpy beds in viscous shearing flows. *Journal of Fluid Mechanics*, 947, A28.
Van Rijn, L.C. (1984a) Sediment transport, Part I: bed load transport. *Journal of Engineering Mechanics*, 110, 1431–1456.
Van Rijn, L.C. (1984b) Sediment transport, Part III: bed forms and alluvial roughness. *Journal of Hydraulic Engineering*, 110(12), 1733–1754. Available from: http://ascelibrary.org/doi/pdf/10.1061/(ASCE)0733-9429(1984)110:12(1733)
Van Rijn, L.C. (1993) Simple general formulae for sand transport in rivers, estuaries and coastal waters. Available from: http://www.leovanrijn-sediment.com/
Vanoni, V.A. (1975) River dynamics. *Advances in applied mechanics*, 15, 1–87.
Wiberg, P.L. & Smith, J.D. (1985a) A theoretical model for saltating grains in water. *Journal of Geophysical Research*, 90, 7341–7354.
Wiberg, P.L. & Smith, J.D. (1985b) A theoretical model for saltating grains in water. *Journal of Geophysical Research: Oceans*, 90(C4), 7341–7354.

How to cite this article: Minster, G., Floc'h, F., Valance, A., Le Dantec, N., Nicolle, A. & Zerr, B. (2024) On the influence of bed roughness on saltation in inertial regime. *Earth Surface Processes and Landforms*, 1–13. Available from: https://doi.org/10.1002/esp.5767